

## Article

# Characterization of Soluplus/ASC-DP Nanoparticles Encapsulated with Minoxidil for Skin Targeting

Rina Takayama <sup>1,2</sup>, Moe Ishizawa <sup>1</sup>, Miyuki Yamada <sup>2</sup>, Yutaka Inoue <sup>1,2,\*</sup>  and Ikuo Kanamoto <sup>2</sup>

<sup>1</sup> Laboratory of Nutri-Pharmacotherapeutics Management, Faculty of Pharmacy and Pharmaceutical Sciences, Josai University, 1-1 Keyakidai, Sakado 3500295, Saitama, Japan; yy15171@josai.ac.jp (R.T.); yy17024@josai.ac.jp (M.I.)

<sup>2</sup> Laboratory of Drug Safety Management, Faculty of Pharmacy and Pharmaceutical Sciences, Josai University, 1-1 Keyakidai, Sakado 3500295, Saitama, Japan; yy13365@josai.ac.jp (M.Y.); kanamoto@josai.ac.jp (I.K.)

\* Correspondence: yinoue@josai.ac.jp; Tel.: +81-49-271-7980

**Abstract:** Soluplus (Sol) is an amphiphilic graft copolymer capable of forming self-assembled micelles and L-ascorbyl 2,6-dipalmitate (ASC-DP) aggregates spontaneously to form micelles. Micelles are used as drug carriers and can nanoparticulate drugs that are poorly soluble in water, such as minoxidil. The study aimed to prepare minoxidil-encapsulated nanoparticles using Sol/ASC-DP and evaluate their potential for targeted skin application. Sol/ASC-DP nanoparticles or Sol/ASC-DP with minoxidil were prepared using the hydration method, and physical evaluations were carried out, including assessments of particle size and zeta potential. Particle structure was evaluated by transmission electron microscopy (TEM) and <sup>1</sup>H-nuclear magnetic resonance spectra to assess particle stability and perform functional evaluations in skin penetration tests. TEM images showed spherical micelle-like particles of approximately 100 nm for Sol/ASC-DP at a 9:1 ratio and of approximately 80 nm for Sol/ASC-DP with incorporated minoxidil at a 9:1:0.5 ratio. Changes were also observed in the solid state, suggesting a hydrophobic interaction between Sol and ASC-DP. In addition, evaporated microparticles (Sol/ASC-DP/minoxidil = 9/1/0.5) improved the skin permeability of minoxidil. These results suggest that Sol/ASC-DP nanoparticles form a stable new nanoparticle due to hydrophobic interactions, which would improve the skin permeability of minoxidil.

**Keywords:** soluplus; L-ascorbyl 2,6-dipalmitate; nanoparticle; minoxidil; permeability



**Citation:** Takayama, R.; Ishizawa, M.; Yamada, M.; Inoue, Y.; Kanamoto, I. Characterization of Soluplus/ASC-DP Nanoparticles Encapsulated with Minoxidil for Skin Targeting. *ChemEngineering* **2021**, *5*, 44. <https://doi.org/10.3390/chemengineering5030044>

Academic Editors: Rajinder Pal and José P. Coelho

Received: 21 June 2021

Accepted: 27 July 2021

Published: 2 August 2021

**Publisher's Note:** MDPI stays neutral with regard to jurisdictional claims in published maps and institutional affiliations.



**Copyright:** © 2021 by the authors. Licensee MDPI, Basel, Switzerland. This article is an open access article distributed under the terms and conditions of the Creative Commons Attribution (CC BY) license (<https://creativecommons.org/licenses/by/4.0/>).

## 1. Introduction

Ultrafine particles or nanoparticles are generally considered to be particles of matter with a diameter of between 1 and 100 nanometers (nm). Nanoparticles are usually classified as microparticles (1–1000 μm) and "fine particles" (100–2500 nm in size). An emulsion is a colloid of two or more immiscible liquids, in which one liquid contains a dispersion of the other. In other words, an emulsion is a specific mixture comprising two liquids that are normally immiscible [1]. Nanoparticles have a variety of physical properties depending on the nanoparticles type, particle size, and composition of the oil and water phases; therefore, nanoparticles are used for different purposes in the food, cosmetics, and pharmaceutical industries [2–4]. However, due to their thermodynamic instability, the preparation of nanoparticles is necessary for the practical use of nanoparticles with long-term stability and convenience [5]. The preparation of particles has become easier with the progress in ultrasonic homogenizers and high-pressure homogenizers [6]. Inoue et al. [7] successfully prepared nanoparticles using an ascorbic acid derivative, trisodium L-ascorbyl 2-phosphate 6-palmitate (APPS), and a surfactant, distearoylphosphatidylethanolamine-PEG2000 (DSPE-PEG (DSPE-PEG2000)), which was used to improve the penetration of the nanoparticles to the skin. Soluplus<sup>®</sup> (Sol) is an amphiphilic block polyvinyl caprolactam-polyvinyl acetate copolymer with a polyethylene glycol (PEG) skeleton as the hydrophilic part and a vinylcaprolactam/vinyl acetate side chain as the hydrophobic part [8]. Sol has

been reported to form self-assembled micelles in an aqueous environment and to improve the solubility of poorly soluble drugs [8,9]. For example, the water solubility of scopoletin (6-methoxy-7-hydroxycoumarin), used for the treatment of rheumatoid arthritis, swelling, and pain, was enhanced by micelle preparation and encapsulation with Sol [10].

In addition, Sol acts as a stabilizer, allowing for the formation of fine and stable particles [9]. Although Sol has been reported to have a low critical micelle concentration and high dispersibility upon dilution, Sol-based nanoparticles have not been developed for many applications to date [11].

Ascorbic acid (ASC) is a water-soluble form of vitamin C with antioxidant properties that is widely used as an additive in foods and pharmaceuticals [12]. ASC also has a whitening effect by reducing pigment deposits and disintegrating melanin and has a wrinkle-reducing effect by stimulating collagen synthesis and improving skin elasticity [13]. However, ASC is sensitive to decomposition and oxidative degradation by heat and light and has low stability. In recent years, a variety of ASC derivatives have been synthesized to improve its stability [14]. One such derivative is L-ascorbyl 6-palmitate (ASC-P), which is characterized by its ability to spontaneously aggregate to form micelles [14]. ASC-P, with the incorporation of hydrophobic groups, is used as a preservative for edible oils and fats, and as an antioxidant for foods [15]. In addition, L-ascorbyl 2,6-dipalmitate (ASC-DP) forms nanoparticles when combined with surfactants without spontaneous aggregation [16]. ASC-DP is used in sunscreen creams and skincare products, and has been studied in the development of cosmetics because of its whitening effects; however, there are few reports of its application in the pharmaceutical field.

We have successfully prepared microparticles by the hydration method using Sol (with amphiphilic properties) and DSPE-PEG2000, which has a PEG-based hydrophilic structure [17]. Therefore, we inferred that Sol and ASC-DP could be used to form finer and more stable particles, which could be applied as drug delivery systems.

Minoxidil (2,4-diamino-6-piperidinopyrimidine-3-oxide) is a pyrimidine derivative and is the most widely used over-the-counter drug for the treatment of male androgenic alopecia [18]. However, there is a concern about the potential cardiovascular side effects of minoxidil since its active metabolite opens vascular smooth muscle ATP-sensitive  $K^+$  channels [19]. If smaller amounts could be selectively transferred to the scalp, the risk of such side effects could be minimized. Toward this end, we hypothesized that microparticles prepared using ASC derivatives and Sol that could encapsulate minoxidil would contribute to expanding the application of minoxidil to the skin.

In this study, we prepared new nanoparticles using ASC derivatives and Sol and evaluated their physicochemical properties and stability. In addition, the therapeutic potential of the nanoparticles encapsulated in minoxidil was investigated by evaluating the skin permeability.

## 2. Materials and Methods

### 2.1. Materials

Sol was provided by BASF Japan Ltd. Tokyo, Japan. ASC-P and ASC-DP were purchased from Tokyo Kasei Kogyo Co., Ltd. Fukaya, Japan. (Figure 1). Minoxidil was purchased from Fujifilm Wako Pure Chemicals Co. Other reagents, including commercial-grade products and NMR solvents, were obtained from Fujifilm Wako Pure Chemicals Co., Ltd. Osaka, Japan.

### 2.2. Sample Preparation

#### 2.2.1. Physical Mixture (PM)

The PM was prepared by weighing Sol/ASC-P or Sol/ASC-DP in different weight ratios (9/1, 8/2, 7/3) and mixed in a vortex mixer for 1 min.

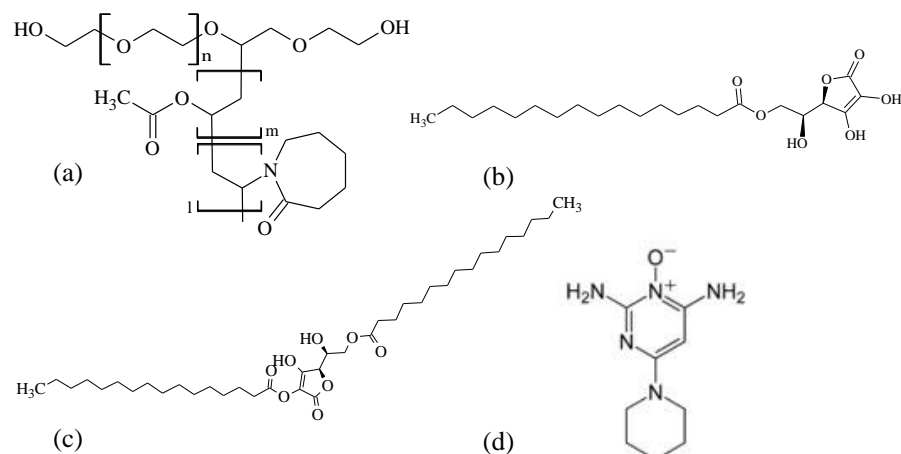


**Figure 1.** Chemical structures of (a) Sol, (b) ASC-P, (c) ASC-DP, and (d) minoxidil.

### 2.2.2. EVP Microparticles

Fine particles were prepared by the hydration method. The hydration method is a process in which each lipid-soluble substance is dissolved in an organic solvent, and the solvent is removed by an evaporator. The prepared thin lipid film is then hydrated in an aqueous solvent to prepare a suspension [16]. Sol, ASC-P, and ASC-DP were prepared at 1 mg/mL using chloroform, and Sol/ASC-P or Sol/ASC-DP was mixed and sonicated in a pear-shaped flask in weight ratios of 9/1, 8/2, and 7/3. Sol was reported to have a critical micelle concentration of 0.82 mg/mL [20]. The EVP Sol was prepared by solvent removal (Rotavapor R-215, Buchi) at 40 °C. Thereafter, the prepared thin film was hydrated with purified water and mixed in a vortex mixer for 1 min, followed by ultrasonication for another 3 min to prepare the particles. Minoxidil-encapsulated particulates were prepared by dissolving minoxidil in methanol (1 mg/mL), and then Sol/ASC-DP/minoxidil was mixed at different weight ratios (9/1/1, 9/1/0.5, 9/1/0.25, 8/2/1, 8/2/0.5, and 8/2/0.25). The particles were prepared by the same procedure using the hydration method. In the stability test, NSS and 5% glucose solution were used in addition to the system prepared with distilled water.

## 2.3. Measurement Methods

### 2.3.1. Particle Size Measurement Using DLS (Dynamic Light Scattering)

The average particle size and polydispersity index (PDI) of the complexes dispersed in water were measured using a Zetasizer Nano ZS system (Malvern Instruments, Malvern, UK). One milliliter of each sample was added to the capillary cell, and the measurement was carried out under Set Zero of 60 s and measurement time of 180 s.

### 2.3.2. Zeta Potential Measurement

Zeta potential measurements were carried out using a Zetasizer Nano ZS system (Malvern Instruments, Malvern, UK) to evaluate the surface charge, which is considered to contribute to the stabilization of particles dispersed in water. One milliliter of each sample was added to the capillary cell, and the measurement was carried out under the conditions of Set Zero of 120 s and measurement time of 180 s.

### 2.3.3. Stability Test

To evaluate the stability of the prepared nanoparticles, they were stored in the absence of light at 25 °C for 10 days. The particle size and zeta potential measurements were performed at intervals of 0, 1, 3, 5, 7, and 10 days as described above.

#### 2.3.4. TEM Measurement

To evaluate the microstructure of the fine particles, TEM measurements were performed using a JEM-2100F microscope (JEOL Co., Ltd. Tokyo, Japan). Hydrophilic treatment of a 200-mesh copper grid covered with a perforated polymer film (Nissin EM Co., Ltd. Tokyo, Japan) was performed with an HDT-400 device (JEOL Co., Ltd.) for 60 s. The outer phase of each suspension was placed in isotonic 290 mM propylene glycol in a size exclusion column. Next, a 2 mL aliquot of each suspension was applied to the hydrophilic grid. The grids were immediately vitrified by absorbing them with filter paper for 3 s and plunging them into liquid ethane cooled with liquid nitrogen in a Leica EM CPC freeze and fix system (Leica Microsystems GmbH, Wetzlar, Germany). The frozen samples were set at approximately  $-170\text{ }^{\circ}\text{C}$  using a Gatan 626 cryo-holder (Gatan Inc. Warrendale, PA, USA). The cryo-TEM system was operated at 120 kV with a nominal magnification of  $50,000\times$ . An under-focus of approximately 2 mm was used to increase the contrast of the images.

#### 2.3.5. PXRD Measurement

To confirm the change in the crystalline state, PXRD measurements were performed using a powder X-ray diffractometer (MiniFlex II, Rigaku). Cu radiation was used as the irradiation dose, and the diffraction intensity was measured using a NaI scintillation counter. The measurements were carried out at 30 kV and 15 mA with a scan speed of  $4^{\circ}/\text{min}$  and a measurement range of  $2\theta = 3\text{--}40^{\circ}$ . The powder sample was packed on a glass plate to ensure that the sample plane was flat. In this study, we performed PXRD measurements on samples in the solid state before hydration.

#### 2.3.6. DSC

To confirm the change in the crystalline state, DSC measurements were performed using a high-sensitivity differential scanning calorimeter (Thermo plus Evo, Rigaku). Approximately 2 mg of the sample was placed in a sealed aluminum pan and measured under a flow rate of 60 mL/min of nitrogen gas at a heating rate of  $5\text{ }^{\circ}\text{C}/\text{min}$ . In this study, we performed DSC measurements on samples in the solid state before hydration.

#### 2.3.7. IR Measurements

NIR measurements were carried out using a Fourier transform NIR spectrometer (NIRFlex N-500, Buchi) to confirm the changes in the intermolecular interactions. The measurement range was  $10,000\text{--}4000\text{ cm}^{-1}$ , the resolution was  $8\text{ cm}^{-1}$ , and the measurement temperature was  $25\text{ }^{\circ}\text{C}$ . The obtained spectra were subjected to a second differential analysis.

IR measurements were performed to confirm the changes in the intermolecular interactions using the potassium bromide (KBr) pellet method. The discs were prepared by mixing the sample with an appropriate amount of KBr and compression-forming by manual pressing. Background correction was performed using a KBr disc alone. The measurement range was  $4000\text{--}650\text{ cm}^{-1}$ , and the resolution was  $4\text{ cm}^{-1}$ . In this study, we performed NIR, IR measurements on samples in the solid state before hydration.

#### 2.3.8. $^1\text{H}\text{--}^1\text{H}$ NOESY NMR Spectroscopy

Two-dimensional NMR measurements were carried out using Varian NMR System 700 MHz (Agilent Technologies, Santa Clara, CA, USA) to confirm the changes in the intermolecular interactions in the solution state. Spectroscopy was measured using an NMR spectrometer (Varian NMR System 700NB, Agilent) with an HCN probe and  $\text{CDCl}_3$  solution operating at 699.7 MHz. The other conditions were a mixing time of 1500 ms, waiting time of 1 s,  $\text{CDCl}_3$  as the solvent, and an integration frequency of 256 at  $25\text{ }^{\circ}\text{C}$ .

#### 2.3.9. Skin Permeability Test

The skin permeation of minoxidil from the minoxidil suspension and the particulate formulation in a uniform preparation volume was evaluated using Yucatan Micropig Skin (YMPs). As a pretreatment, skin of YMPs (5 months old, female) that had been frozen at

−80 °C was thawed at 4 °C for about 12 h before use. After thawing, the subcutaneous fat was removed, and the skin was cut into approximately 2.5 × 2.5 cm pieces. The stratum corneum was removed by tape-stripping 30 times. The treated YMP skin was approximately 2–3 mm thick. After removal of the stratum corneum, the YMP skin was placed epidermis side up on a paper towel moistened with NSS and stored at 4 °C for 12 h. The efficacy and safety of locally acting drugs applied on skin are determined by their distribution into its intended site of action, the viable epidermis and dermis (VED), and not the stratum corneum (SC). Hence, tape-stripping was completed. A Franz-type diffusion cell (Perme Gear, effective penetration area: approximately 0.95 cm<sup>2</sup>) was used for the permeability test following the method described by [21–23]. The receiver phase was filled with approximately 9.5 mL of phosphate-buffered saline (pH 7.4; Thermo Fisher Scientific Life Technology Japan Inc. Osaka, Japan). During the permeation test, the receiver phase was agitated at 32 ± 2 °C. The YMP skin was placed on a Franz-type diffusion cell with the epidermis side facing the donor compartment with the dermis side towards the receiver. In the donor compartment, 2 mL of minoxidil suspension and the prepared microparticle formulation were applied. The receiver solution was continuously stirred with a magnetic stirrer throughout the experiment. At predetermined times (1, 3, 6, 24 h), an aliquot (0.5 mL) was withdrawn from the receiver solution, and the same volume of PBS was added to keep the volume constant. After 24 h, the YMP skin was demounted from the Franz diffusion cell, the epidermal side was gently washed with NSS, and then the effective area was cut into small pieces. The finely diced YMP skin was homogenized (26,000 rpm, 2 min) using POLYTRON<sup>®</sup>PT-MR2500 by adding 2 mL of methanol to 0.2 g of skin. The homogenized samples were centrifuged (25 °C, 2600 × g, 30 min) and the supernatant was further centrifuged (4 °C, 20,000 × g, 10 min) and passed through a 0.45 µm membrane filter. The determination of minoxidil in YMP skin was performed using a Waters 2795 UV-visible spectrophotometer (Waters Japan Co., Ltd. Shinagawa, Japan) under the following conditions: wavelength, 230 nm; Inertsil<sup>®</sup> ODS-3 column (5 µm diameter, 4.6 × 150 mm; GL Sciences Inc. Tokyo, Japan.); column temperature, 40 °C; mobile phase, water/methanol = 2/1; injection volume, 50 µL; retention time, adjusted to approximately 7 min (minoxidil).

### 3. Results and Discussion

#### 3.1. Evaluation of Sol/ASC-DP Particles

##### 3.1.1. Particle Size and Zeta Potential Measurement

Particle size and zeta potential measurements were performed to evaluate the validity of the particulate preparation. Sol has a surfactant effect and therefore exhibits micelle properties; the hydrophobic tails of several surfactant molecules assemble into an oil-like core, the most stable form of which had no contact with water. We measured the particle size by dynamic light scattering. Dynamic light scattering particle size analyzers are used to measure the size of very small particles (0.6 nm to 6 µm) in the solution. This class of particle size analyzer interprets particles' sizes from the fluctuations in scattered laser light created by the particles' Brownian motion. The particle size and zeta potential measurements are presented in Figure 2. Sol alone had an average particle size of 63.8 nm (zeta potential: approximately −8.6 mV) and showed a single distribution peak (Figure 2a). ASC-P alone had an average particle size of 2948 nm (zeta potential: approximately −46.8 mV), and ASC-DP alone had an average particle size of 1191 nm (zeta potential: approximately −7.3 mV); particles that appeared to be aggregated were observed after 1000 nm (Figure 2b,f).

The samples were then prepared in mixed weight ratios (Sol/ASC-P = 9/1, 8/2, 7/3 and Sol/ASC-DP = 9/1, 8/2, 7/3), and their particle size and zeta potential were evaluated. Particles that were considered to be aggregated after 1000 nm were measured for all mixing ratios of Sol/ASC-P, as well as for ASC-P alone (Figure 2c–e). Sol/ASC-DP at 9/1 had an average particle size of 81.1 nm (zeta potential: approximately −19.5 mV), Sol/ASC-DP at 8/2 had an average particle size of 101.5 nm (zeta potential: approximately −21.2 mV), and Sol/ASC-DP at 7/3 had an average particle size of 169.3 nm (zeta potential:

approximately  $-23.0$  mV). Therefore, the particle size tended to increase as the weight ratio of ASC-DP increased.

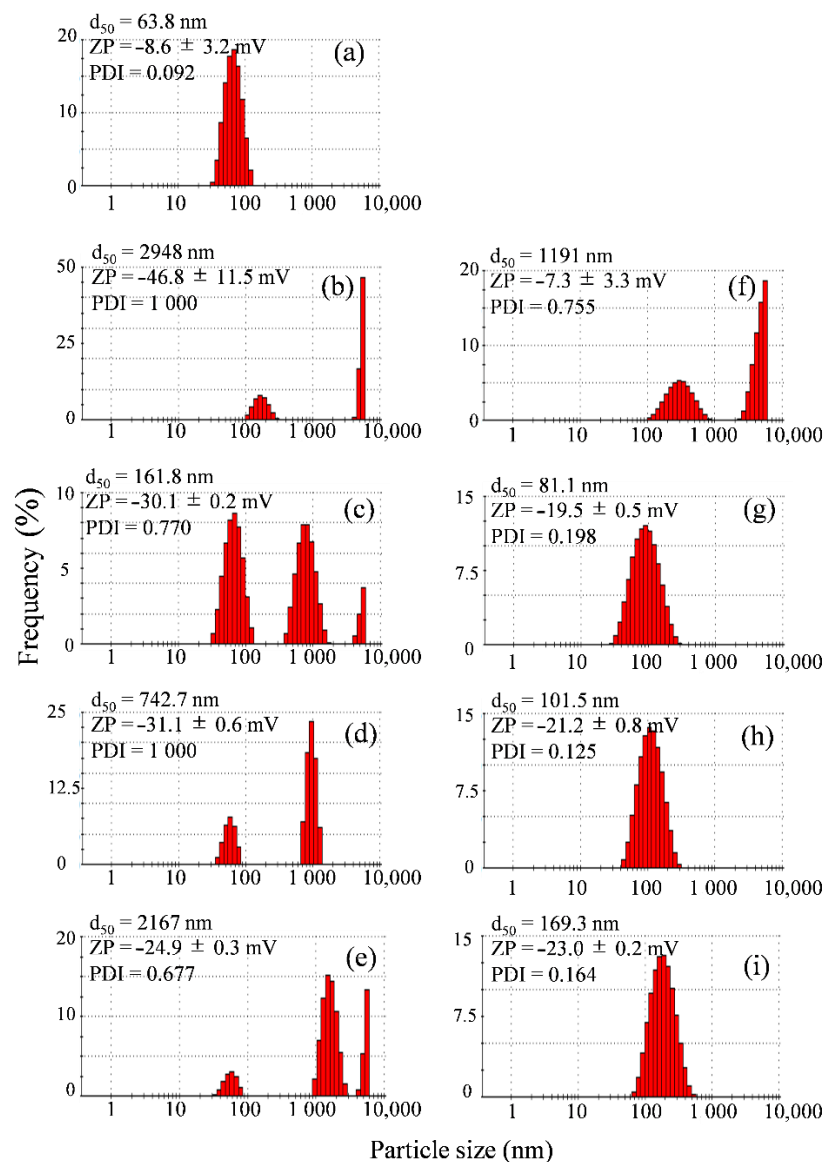


**Figure 2.** Particle size patterns and zeta potential of (a) Sol, (b) ASC-P, (c) Sol/ASC-P (9/1), (d) Sol/ASC-P (8/2), (e) Sol/ASC-P (7/3), (f) ASC-DP, (g) Sol/ASC-DP (9/1), (h) Sol/ASC-DP (8/2), and (i) Sol/ASC-DP (7/3). Zeta potential represents the mean  $\pm$  S.D. ( $n = 3$ ).

The zeta potential also exhibited a similar tendency wherein it increases as the mixing weight ratio of ASC-DP increased. From these findings, it was assumed that intermolecular interactions between ASC-DP and Sol contributed to the particle size because particle aggregation was observed when ASC-DP was used alone but was suppressed when ASC-DP was mixed with Sol. As the zeta potential also changed with different mixing weight ratios of Sol/ASC-DP, it can be inferred that the mixing weight ratio affects the stability of the particles. A high zeta potential (20 mV or more) prevents aggregation, as particles are repelled from each other by their surface charge. In general, it has been reported that the zeta potential provides stability to particles at 20–30 mV [24]; therefore, it is presumed that the prepared particles are relatively stable. Based on these results, we then investigated the optimal mixing weight ratio by conducting stability tests of Sol/ASC-DP particles.

### 3.1.2. Stability Test

The stability of the suspensions prepared at various weight ratios (Sol/ASC-DP = 9/1, 8/2, 7/3) was evaluated at 25 °C for 10 days in the absence of light (Figure 3). No significant change in the average particle size for particles prepared at any ratio was observed until day 7. However, an increase in particle size was observed on day 10. This suggests that the particles became unstable due to aggregation and dissociation only after the tenth day. The fact that the particles were relatively stable for 7 days after hydration suggests that they can be used in injectable formulations. However, we wondered why the particles could be prepared in distilled water, and whether the particle surface charge might contribute to the stability of the particles. We used normal saline solution (NSS) and 5% glucose (5%G) solution and examined the stability through their changes in particle size and zeta potential.

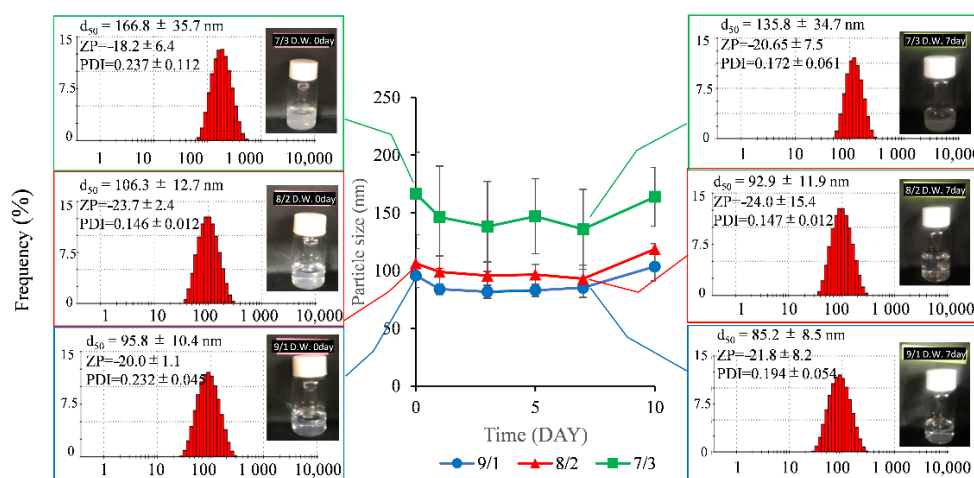


**Figure 3.** Changes in particle size and zeta potential of nanoparticles of Sol/ASC-DP at mixing ratios of 9/1, 8/2, and 7/3 after storage at 25 °C from day 0 to day 10 in distilled water. Zeta potential is presented as the mean  $\pm$  S.D. ( $n = 3$ ).

Therefore, stability tests were conducted under the same conditions for suspensions hydrated with normal saline solution (NSS) and 5% glucose solution (5% G), which are commonly used as dissolution solutions for injectable drugs (Figures 4 and 5). When hydrated with NSS, aggregated particles of approximately 1,000 nm or more were observed for Sol/ASC-DP of 8/2 and 7/3 on day 0. For Sol/ASC-DP of 9/1, the average particle size increased gradually from 139.4 nm on day 0, and the particle size became polydisperse on day 7. By contrast, when Sol/ASC-DP of 9/1, 8/2, and 7/3 was hydrated using 5% G, no significant change in the average particle size was observed until day 7. Based on this finding, it was estimated that hydration with 5% G would provide more stable particles when using Sol/ASC-DP as an injectable. In addition, the particle size showed a tendency to increase as the mixing weight ratio of ASC-DP increased, even when the dispersion solution was different, suggesting that 9/1 Sol/ASC-DP is a stable mixing ratio. Slightly precipitated particles visually confirmed the origin of the peak above 1000 nm out of the DLS range. In the NSS dispersion, it was confirmed that the zeta potential and PDI values decreased with the lapse of the observation period. We speculated that this was due to salting out of the saline solution. In distilled water and 5% glucose, the particle size measurement seems to be stable for 7 days, but when we checked the Auto Correlation Function of DLS, the scattering intensity of Sol/ASC-DP = 7/3 in the solvent decayed quickly, and we observed the existence of large particles (data not shown). Therefore, the mixing ratio of Sol/ASC-DP = 8/2 or 9/1 was considered appropriate. Generally, the surface of particles has an electric charge, and aggregation between particles is suppressed by electrostatic repulsion due to the surface charge. However, in the case of NSS, it is

considered that the decrease in zeta potential on the particle surface is due to sodium and chloride ions affecting the stability.

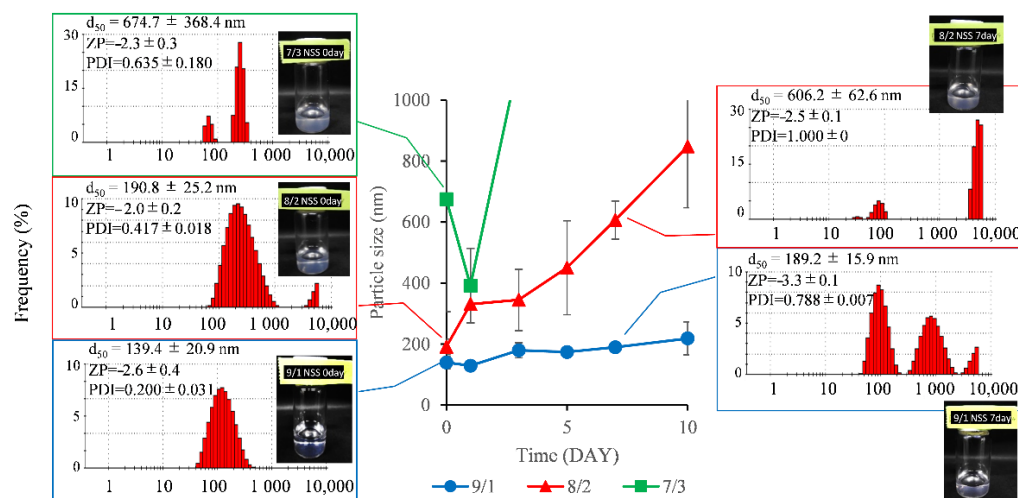


**Figure 4.** Changes in particle size and zeta potential of nanoparticles of Sol/ASC-DP at mixing ratios of 9/1, 8/2, and 7/3 after storage at 25 °C from day 0 to day 10 in saline. Zeta potential is presented as mean  $\pm$  S.D. ( $n = 3$ ).

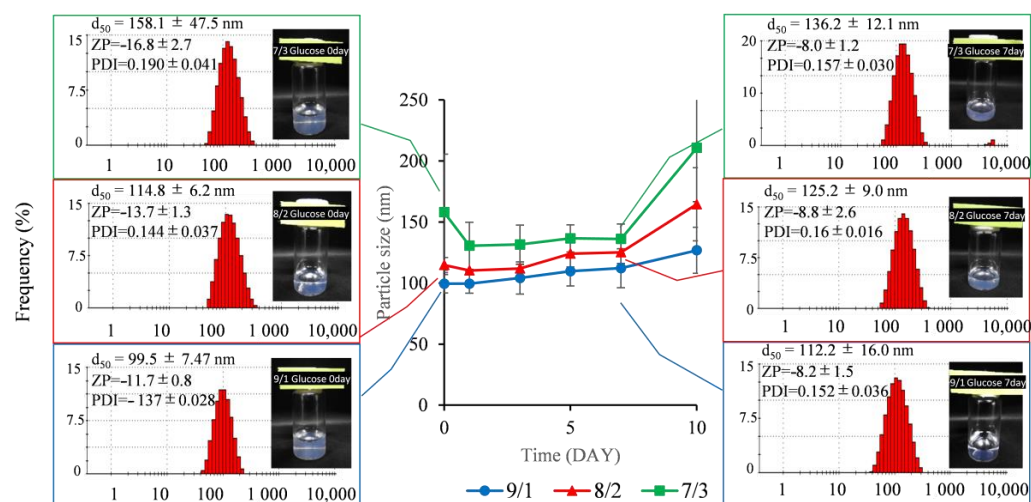


**Figure 5.** Changes in particle size and zeta potential of nanoparticles of Sol/ASC-DP at mixing ratios of 9/1, 8/2, and 7/3 after storage at 25 °C from day 0 to day 10 in 5% glucose solution. Zeta potential is shown as mean  $\pm$  S.D. ( $n = 3$ ).

### 3.1.3. Transmission Electron Microscopy (TEM) Measurement

From the results of the above stability tests and confirmation of particle formation in different solvents using Sol/ASC-DP = 7/3, 8/2, and 9/1, we inferred that a Sol/ASC-DP ratio of 8/2 or 9/1 would be appropriate, so we were interested in the particle shape and conducted TEM measurements. To observe the morphology of the prepared nanoparticles, TEM measurements were performed on the suspensions with Sol/ASC-DP at 9/1 and 8/2 mixing ratios (Figure 6). Particles of approximately 100 nm were observed for Sol/ASC-DP of 9/1 and 8/2, which is consistent with the results of the particle size measurement. The particles showed a circular shape. When the particles had a liposome, bi-layer structure, a lamellar structure was observed [25]. However, the newly prepared Sol/ASC-DP particles at ratios of 9/1 and 8/2 did not show any lamellar structure. Moribe et al. previously reported the micelle formation in DSPE-PEG and ASC derivatives [16]. A liposome is a spherical-shaped vesicle that is composed of one or more phospholipid bilayers as lamellar

structure, which closely resembles the structure of cell membranes. Generally, double-membrane structures, such as liposomes, form lamellar structures [25]. We also concluded that these particles had a micelle-like structure because no lamellar structure was observed, and TEM images showed a distinct characteristic from liposomes. Based on this previous finding, we speculated that Sol/ASC-DP also has a micelle-like structure.

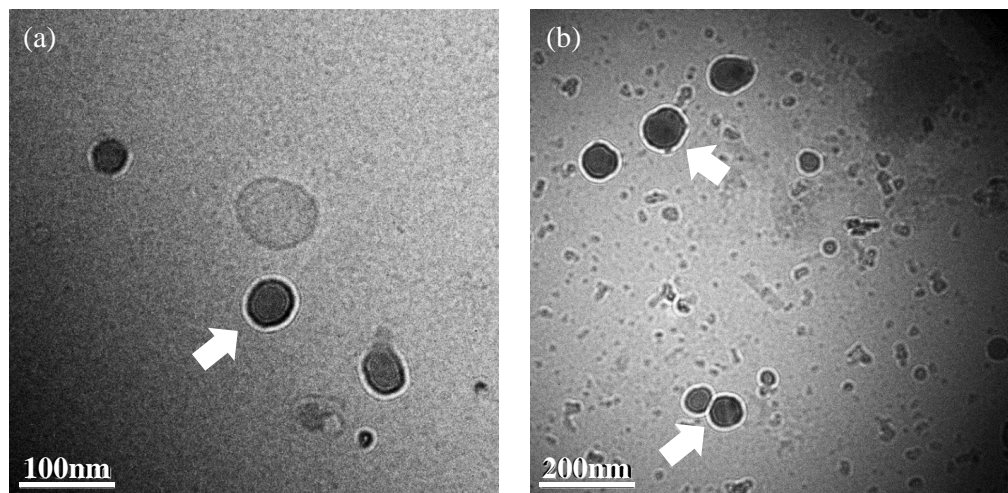


**Figure 6.** TEM images of nanoparticles. (a) Sol/ASC-DP = 9/1, (b) Sol/ASC-DP = 8/2.

### 3.2. Evaluation in Solid State

#### 3.2.1. Powder X-ray Diffraction (PXRD) Measurement

The formation of fine particles was confirmed by preparing Sol/ASC-DP using the hydration method. It is suspected that the solid state formed at the time of hydration would affect particle formation. Possibly, we thought that ASC-DP and Sol might have already interacted with each other in the solid state before hydration. Therefore, PXRD measurements were performed to confirm the change in the crystal structures in the solid state (Figure 7). Sol did not reveal any characteristic diffraction peaks, indicating a halo pattern. ASC-DP showed characteristic diffraction peaks (open circles in Figure 7) around  $2\theta = 3.7^\circ, 5.6^\circ, 18.9^\circ,$  and  $20.6^\circ$ . Similarly, evaporated (EVP) Sol showed a halo pattern, and EVP (ASC-DP) showed diffraction peaks derived from ASC-DP at around  $2\theta = 3.7^\circ, 5.5^\circ, 18.9^\circ,$  and  $20.4^\circ$ . In the physical mixture (PM; Sol/ASC-DP = 9/1, 8/2), ASC-DP-derived diffraction peaks were observed at  $2\theta = 3.7^\circ, 5.6^\circ, 18.9^\circ,$  and  $20.6^\circ$ , whereas in EVP (Sol/ASC-DP = 9/1, 8/2), the characteristic diffraction peaks disappeared and a halo pattern was observed. The ground mixture of clarithromycin and L-ascorbic acid 2-glucoside was reported to be amorphous in PXRD measurements and is known to form fine particles when the sample is dispersed in distilled water [26]. Therefore, it is speculated that EVP (Sol/ASC-DP = 9/1, 8/2) might also contain microcrystals that were not observed in the PXRD measurements.

#### 3.2.2. Differential Scanning Calorimetry (DSC) Measurement

DSC measurements were further performed to confirm the thermal behavior of the particles in solid state (Figure 8). Endothermic peaks derived from the melting point of ASC-DP were observed at approximately  $58^\circ\text{C}, 96^\circ\text{C},$  and  $114^\circ\text{C}$ . In PM (Sol/ASC-DP = 9/1), an endothermic peak derived from the melting point of ASC-DP was observed at approximately  $58^\circ\text{C}$ , and in PM (Sol/ASC-DP = 8/2), the endothermic peak derived from the melting point of ASC-DP was observed at approximately  $58^\circ\text{C}, 96^\circ\text{C},$  and  $114^\circ\text{C}$ , respectively. Interestingly, in EVP (Sol/ASC-DP = 9/1, 8/2), the endothermic peak derived from the melting point of ASC-DP disappeared. In the exothermic peaks mean in the DSC thermograms Figure 8d,e, the exothermic peaks, due to the decomposition of Sol, were observed at around  $250^\circ\text{C}$  and  $270^\circ\text{C}$ . This suggests that some type of interaction between

Sol and ASC-DP may have occurred, leading to the dispersed coordination of ASC-DP in the solid dispersion of Sol.

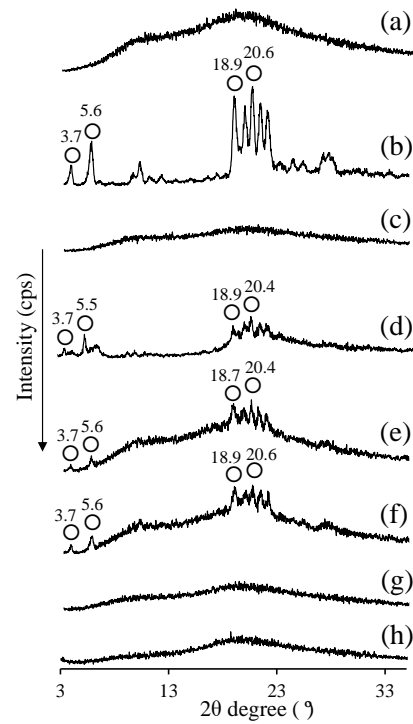


**Figure 7.** PXRD patterns of Sol/ASC-DP systems. (a) Sol, (b) ASC-DP, (c) EVP (Sol), (d) EVP (ASC-DP), (e) PM (Sol/ASC-DP = 9/1), (f) PM (Sol/ASC-DP = 8/2), (g) EVP (Sol/ASC-DP = 9/1), and (h) EVP (Sol/ASC-DP = 8/2). ○: ASC-DP diffraction peaks.

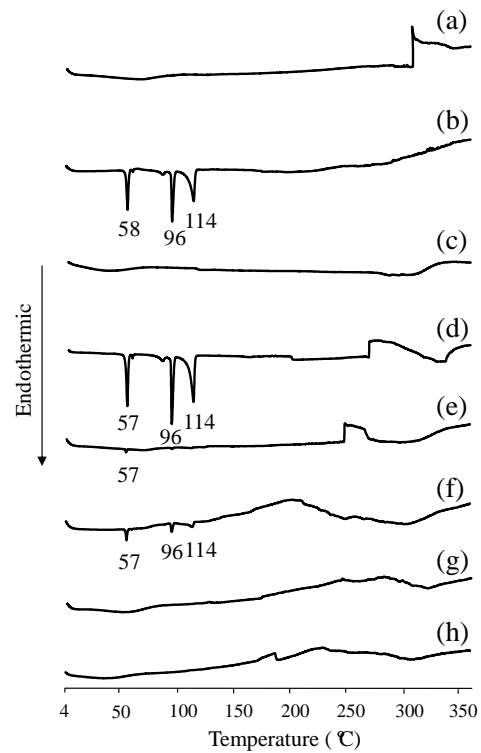


**Figure 8.** DSC curves of Sol/ASC-DP systems. (a) Sol, (b) ASC-DP, (c) EVP (Sol), (d) EVP (ASC-DP), (e) PM (Sol/ASC-DP = 9/1), (f) PM (Sol/ASC-DP = 8/2), (g) EVP (Sol/ASC-DP = 9/1), and (h) EVP (Sol/ASC-DP = 8/2).

### 3.2.3. Near-Infrared (NIR) Measurement

NIR and IR measurements are useful methods to verify drug–drug intermolecular interactions in the solid state in the preparation of particulates. NIR absorption spectroscopy was performed to confirm the intermolecular interaction of Sol/ASC-DP (Figure 9). In the EVP (Sol/ASC-DP), the peaks of the CH group at around  $5844\text{ cm}^{-1}$  and  $8260\text{ cm}^{-1}$ , which are considered to be derived from Sol, were found to be shifted. This suggests that the interaction of Sol with CH groups, likely derived from PEG, contributed to the formation of particles.

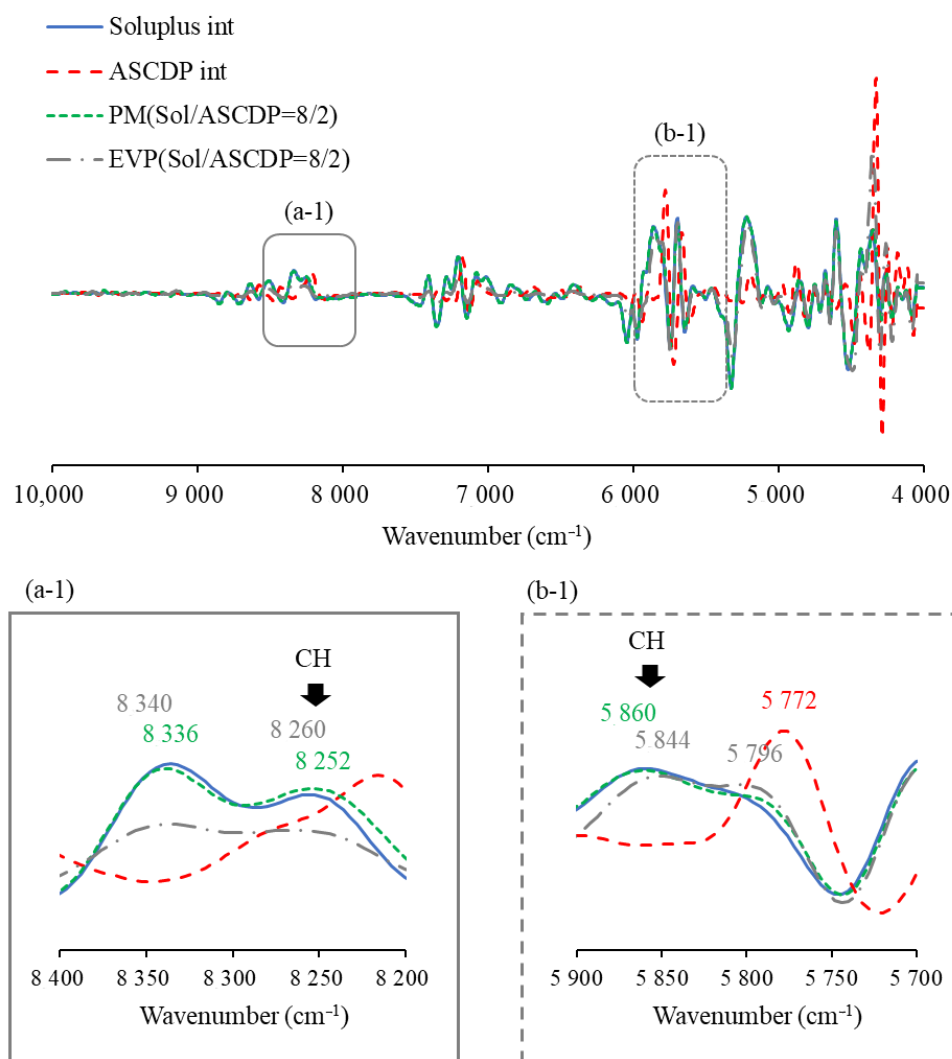


**Figure 9.** Second-differentiation NIR absorption spectra of Sol/ASC-DP systems. (a-1)  $8400\text{--}8200\text{ cm}^{-1}$ , (b-1)  $5900\text{--}5700\text{ cm}^{-1}$ .

### 3.2.4. Infrared (IR) Measurement

We then measured IR absorption spectra to confirm the intermolecular interactions of carbonyl groups that were not confirmed by NIR measurements (Figure 10). In EVP (Sol/ASC-DP), the  $1674\text{ cm}^{-1}$  peak derived from the carbonyl group of ASC-DP disappeared, and a new peak at approximately  $1771\text{ cm}^{-1}$  was identified. In EVP (Sol/ASC-DP), the  $1740\text{ cm}^{-1}$  peak derived from the carbonyl group of the lactone ring of ASC-DP was broadened. In addition, the peak at  $3455\text{ cm}^{-1}$ , derived from the hydroxyl group of ASC-DP, disappeared. The sharp peak at  $2960\text{--}2840\text{ cm}^{-1}$  derived from the CH group of ASC-DP was broadened in EVP (Sol/ASC-DP). Therefore, EVP (Sol/ASC-DP) may have intermolecular interactions due to hydrogen bonding in the solid state.

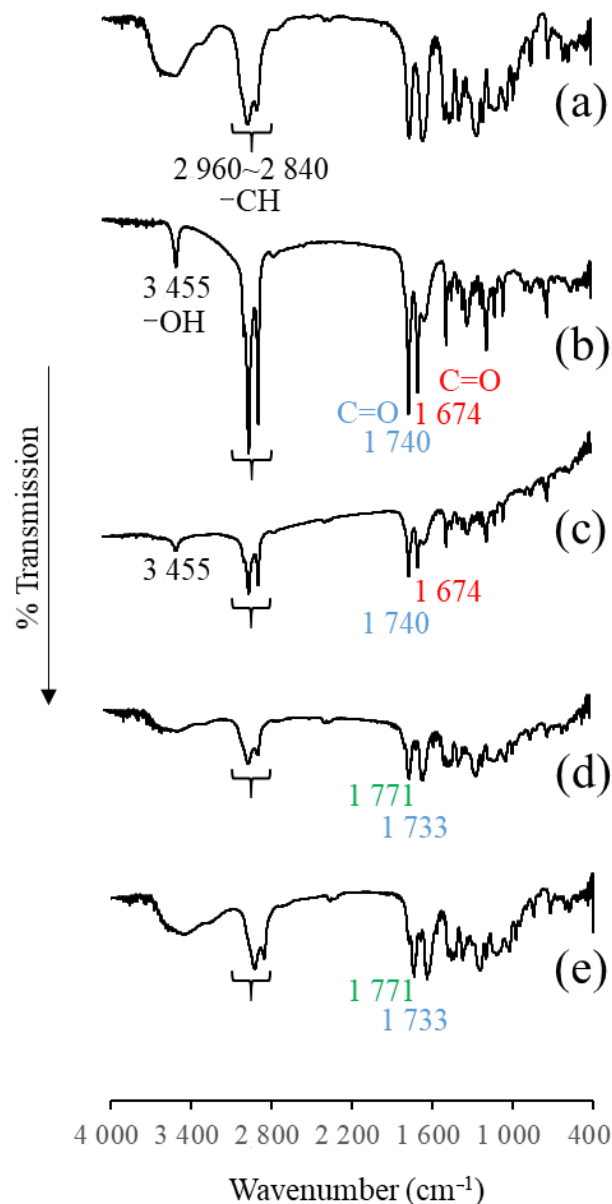


**Figure 10.** FT-IR absorption spectra of Sol/ASC-DP systems. (a) Sol, (b) ASC-DP, (c) PM (Sol/ASC-DP = 8/2), (d) EVP (Sol/ASC-DP = 9/1), (e) EVP (Sol/ASC-DP = 8/2).

### 3.3. Evaluation in Liquid State

#### NOESY NMR Measurement

To examine the intermolecular interactions in detail,  $^1\text{H}$ - $^1\text{H}$ -NOESY NMR measurements were performed (Figure 11). The ASC-DP peak attribution was based on the ASC peak attribution reported by Kurata et al. [27]. The PEG-derived  $\text{CH}_2$  group X of Sol (1.5–1.8 ppm) showed a cross peak with the CH group a (4.8 ppm) derived from the 4-position of the lactone ring of ASC-DP, and with b and c (4.7 ppm) derived from the 5- and 6-positions. This suggests that hydrophobic intermolecular interactions via hydrogen bonding may have occurred at the 4-, 5-, and 6-positions of the PEG moiety of Sol and the lactone ring of ASC-DP. These findings suggest that Sol/ASC-DP is stable in water.

Considering that stable microparticles were formed in Sol/ASC-DP, we prepared microparticles in a three-component system: Sol/ASC-DP with incorporated minoxidil.

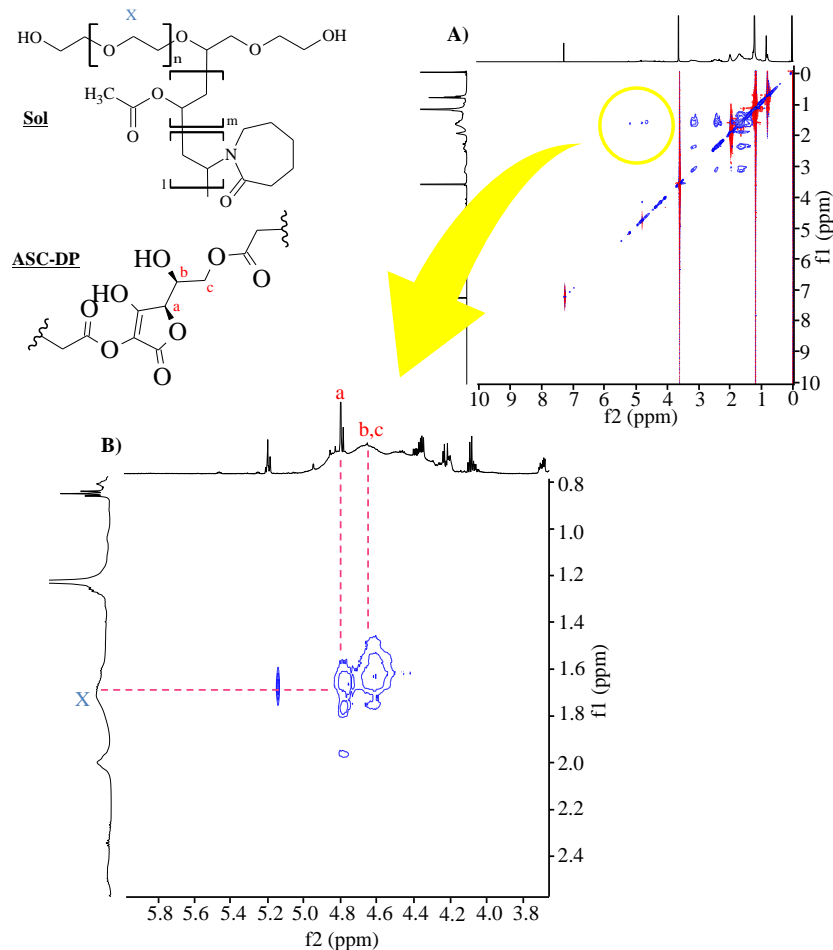


**Figure 11.**  $^1\text{H}$ - $^1\text{H}$  NOESY NMR spectra EVP (Sol/ASC-DP = 8/2) in  $\text{CDCl}_3$ . (A)  $f_1$  is 0–10 ppm;  $f_2$  is 0–10 ppm. (B)  $f_1$  is 1.4–1.8 ppm;  $f_2$  is 4.5–4.8 ppm.

### 3.4. Evaluation of Sol/ASC-DP/Minoxidil Particles Particle Size and Zeta Potential Measurement

Particle size and zeta potential measurements were performed to evaluate the stability of nanoparticle preparations (Figure 12). In the case of Sol/ASC-DP/minoxidil at 9/1/1, 8/2/1, and 8/2/0.5, particles were considered to be aggregated around 1000 nm (Figure 12a,b,d). However, for Sol/ASC-DP/minoxidil at 9/1/0.5, 9/1/0.25, and 8/2/0.25, a single distribution peak at approximately 100 nm was observed (Figure 12c,e,f). Sol/ASC-DP/minoxidil at 9/1/0.5 had an average particle size of 80.3 nm (zeta potential: approximately  $-19.7$  mV), and Sol/ASC-DP/minoxidil at 9/1/0.25 had an average particle size of 75.0 nm (zeta potential: approximately  $-20.5$  mV). Therefore, the smaller the weight ratio of minoxidil, the smaller the average particle size. The average particle size of Sol/ASC-DP/minoxidil at 8/2/0.25 was 124.2 nm (zeta potential: approximately  $-23.1$  mV), and it was confirmed that both the average particle size and zeta potential were larger than those of the system with a Sol/ASC-DP ratio of 9/1 with minoxidil. In the mixture ratio of Sol/ASC-DP/Minoxidil = 9/1/0.5, the particle size was about 75.0 nm (zeta potential: approximately  $-20.5$  mV). In general, when the zeta potential is about  $-20$  mV, the particles are inhibited by electrostatic repulsion, which suppresses particle aggregation [24], and we thought that stable particle formation was possible. The particle size of Sol/ASC-DP/minoxidil = 8/2/0.25 was about 100 nm, and the zeta potential was about  $-23$  mV, suggesting that stable microparticles were prepared. Though, the content of minoxidil is half that of Sol/ASC-DP/Minoxidil = 9/1/0.5. Therefore, Sol/ASC-DP/Minoxidil = 9/1/0.5 was used for the skin permeation test.

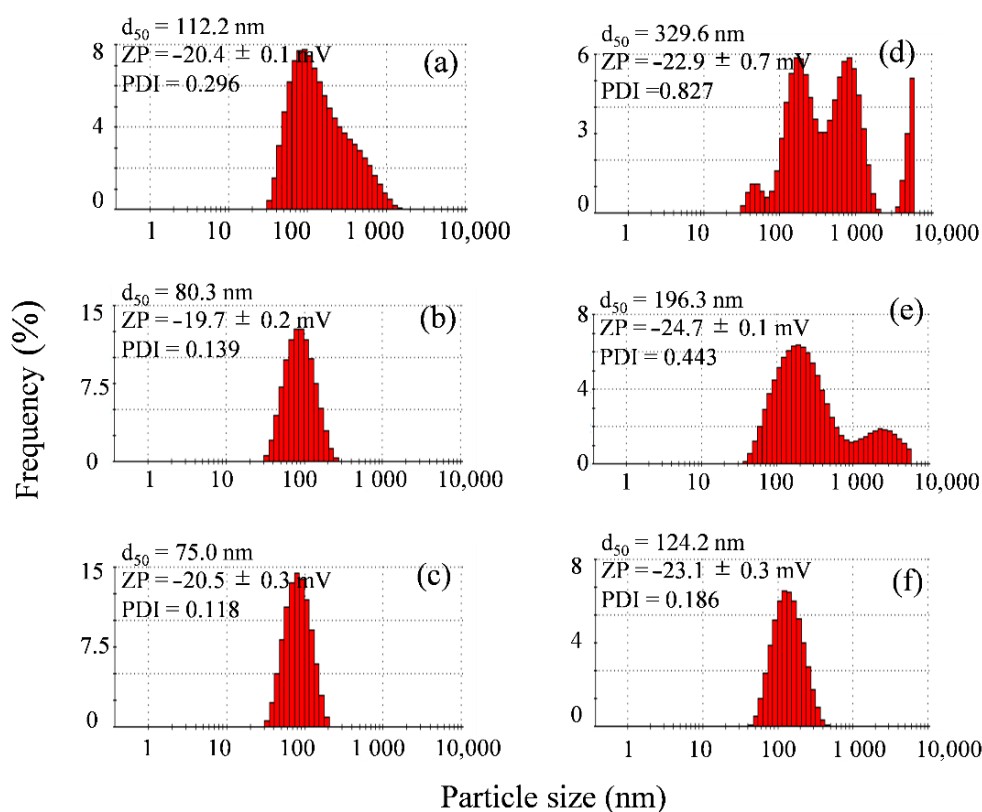


**Figure 12.** Particle size patterns and zeta potential of Sol/ASC-DP/minoxidil systems at different ratios. (a) Sol/ASC-DP/minoxidil = 9/1/1, (b) Sol/ASC-DP/minoxidil = 9/1/0.5, (c) Sol/ASC-DP/Minoxidil = 9/1/0.25, (d) Sol/ASC-DP/minoxidil = 8/2/1, (e) Sol/ASC-DP/minoxidil = 8/2/0.5, (f) Sol/ASC-DP/minoxidil = 8/2/0.25. Zeta potential: mean  $\pm$  S.D. ( $n = 3$ ).

### 3.5. Evaluation of Skin Adaptation

#### Skin Permeation Test

Skin permeation studies on the skin of YMPs were conducted to compare the efficacy of the minoxidil suspension alone and EVP (Sol/ASC-DP/minoxidil = 9/1/0.5), a fine particle formulation containing minoxidil (Figure 13). Minoxidil was not detected in the receiver solution, indicating that the drug did not penetrate the skin. It was confirmed that  $0.19 \pm 0.01 \mu\text{g}/\text{cm}^2$  of the minoxidil suspension remained in the skin, whereas  $0.32 \pm 0.07 \mu\text{g}/\text{cm}^2$  remained on the skin after the application of EVP (Sol/ASC-DP/minoxidil = 9/1/0.5). This suggested that the particulate formulation is an effective method for delivering minoxidil into the skin. Moribe et al. [16] reported the preparation of fine particles by DSPE-PEG/ASC-DP, and we reported the preparation of fine particles by DSPE-PEG/Sol [17]. Notably, in the present study, Sol/ASC-DP enabled the preparation of microparticles, thus further expanding the application of encapsulating minoxidil to the skin. Therefore, the nanoparticulate formulation utilizing Sol/ASC-DP is considered to be an effective means for the efficient delivery of drugs into the skin. Thus, skin drug permeation studies were conducted using Sol/ASC-DP/Minoxidil = 9/1/0.5. In the presence of Sol/ASC-DP nanoparticles, the concentration of minoxidil in the skin increased by 68%, which is about 1.5 times higher than that of minoxidil alone. The clinical efficacy of this minoxidil delivery is not sufficiently proposed in this study. It is an important issue to be verified by in vivo studies in the future. The clinical application of minoxidil-containing nanoparticles must also be assessed carefully, not only for efficacy but also for side effects.

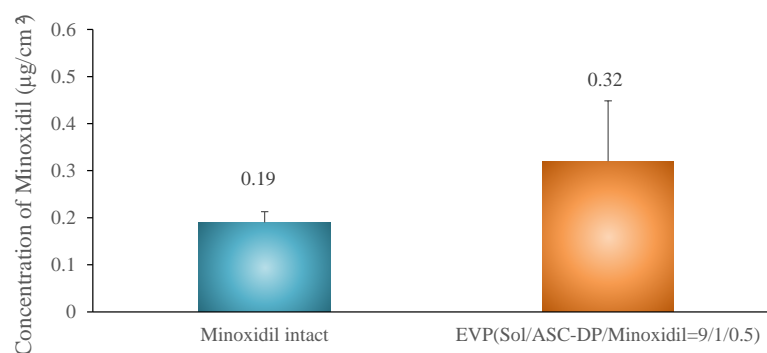


**Figure 13.** Cumulative amount of transdermal minoxidil after 24 h.

However, the detailed formation mechanism and structure of the nanoparticles are not yet fully determined and are subjects for further investigation in the future. The preparation of drug–nanoparticle complexes must be evaluated for their toxicity and kinetic properties to integrate their use in drug formulation and clinical practice.

#### 4. Conclusions

Sol/ASC-DP prepared using the hydration method at mixture ratios of 9/1 and 8/2 formed stable new nanoparticles by hydrophobic interactions. The particles were observed to be stable for 7 days under light-shielded conditions at 25 °C. The particles hydrated with 5% G were also stable for 7 days under the same conditions. TEM observations showed spherical micelle-like particles of approximately 100 nm at Sol/ASC-DP with ratios of 9/1 and 8/2. Changes were also observed in PXRD, DSC, NIR, and IR measurements in the solid state, suggesting the possibility of some interaction between Sol and ASC-DP. The findings of the skin permeability test and TEM observations of minoxidil nanoparticles enhanced the delivery of the drug into the skin. In this study, it was confirmed that the interaction of ASC-DP with Sol not only improved its dispersibility in water but also resulted in the formation of nanoparticles, even though ASC-DP is an insoluble vitamin C derivative. We believe that the nanoparticle formation suggests that there may be some interaction between Sol and ASC-DP, which will provide useful information for other researchers to study nanoparticles in the future.

**Author Contributions:** Conceptualization, methodology, analysis, investigation, and original draft preparation, R.T. and Y.I.; analysis and investigation, M.I. and M.Y.; validation, M.I.; writing—review and editing, R.T., I.K. and Y.I.; methodology, supervision, resources, project administration, and original draft preparation, Y.I. All authors have read and agreed to the published version of the manuscript.

**Funding:** This research was supported by Josai University.

**Institutional Review Board Statement:** Not applicable.

**Informed Consent Statement:** Not applicable.

**Acknowledgments:** The authors wish to thank BASF Japan Ltd. and Soluplus and Hiroaki Todo, at the Faculty of Pharmacy and Pharmaceutical Sciences, Josai University, Japan, for providing support for the skin permeability study. We thank Kenjiro Higashi, at Chiba University, Japan, for his kind advice and expert TEM measurements, and especially for his perspectives in applied science, which encouraged us to undertake this study. We also thank the Graduate School of Pharmaceutical Sciences, Chiba University, Japan, for the TEM measurements.

**Conflicts of Interest:** The authors declare that there are no conflicts of interest regarding the publication of this paper.

## Abbreviations

5% G, 5% glucose solution; ASC-DP, L-ascorbyl 2,6-dipalmitate; ASC-P, L-ascorbyl 6-palmitate; DSC, differential scanning calorimetry; EVP, evaporated; NIR, near-infrared; NSS, normal saline solution; PDI, phase Doppler interferometer; PEG, polyethylene glycol; PM, physical mixture; PXRD, powder X-ray diffractometers; Sol, Soluplus; TEM, transmission electron microscopy; YMP, Yucatan micropig.

**Sample Availability:** Samples of the compounds are not available from the authors.

## References

1. Clayton, W. *Theory of Emulsions*, 4th ed.; Blackston Co.: New York, NY, USA, 1943.
2. Ito, M.; Uehara, M.; Wakui, R.; Shiota, M.; Kuroiwa, T. Preparation Characteristics of Water-in-oil Emulsion Using Olive Oil as a Continuous Phase in Microchannel Emulsification. *Jpn. J. Food Eng.* **2017**, *18*, 103–111. (In Japanese) [[CrossRef](#)]
3. Suzuki, R.; Takizawa, T.; Kuwata, Y.; Mutoh, M.; Ishiguro, N.; Utoguchi, N.; Shinohara, A.; Eriguchi, M.; Yanagie, H.; Maruyama, K. Effective Anti-Tumor Activity of Oxaliplatin Encapsulated in Transferrin-PEG-Liposome. *Int. J. Pharm.* **2008**, *346*, 143–150. [[CrossRef](#)] [[PubMed](#)]
4. Onoue, S.; Yamada, S.; Chan, H.K. Nanodrugs: Pharmacokinetics and Safety. *Int. J. Nanomed.* **2014**, *9*, 1025–1037. [[CrossRef](#)]
5. Chen, H.; Khemtong, C.; Yang, X.; Chang, X.; Gao, J. Nan-onization Strategies for Poorly Water-Soluble Drugs. *Drug Discov.* **2010**, *16*, 354–360.
6. Morita, M.; Katada, M. Preparation of O/W Emulsions by High Pressure Homogenizer. *J. Jpn. Oil Chem. Soc.* **1991**, *40*, 58–63. [[CrossRef](#)]
7. Inoue, Y.; Hibino, M.; Murata, I.; Kanamoto, I. A Nanocarrier Skin-Targeted Drug Delivery System Using an Ascorbic Acid Derivative. *Pharm. Res.* **2017**, *35*, 1–14. [[CrossRef](#)]
8. Kataoka, K.; Harada, A.; Nagasaki, Y. Block Copolymer Micelles for Drug Delivery: Design, Characterization and Biological Significance. *Adv. Drug Deliv. Rev.* **2012**, *64*, 37–48. [[CrossRef](#)]
9. Yang, H.; Teng, F.; Wang, P.; Tian, B.; Lin, X.; Hu, X.; Zhang, L.; Zhang, K.; Zhang, Y.; Tang, X. Investigation of a Nano-suspension Stabilized by Soluplus<sup>®</sup> to Improve Bioavailability. *Int. J. Pharm.* **2014**, *477*, 88–95. [[CrossRef](#)] [[PubMed](#)]
10. Zeng, Y.C.; Li, S.; Liu, C.; Gong, T.; Sun, X.; Fu, Y.; Zhang, Z.R. Soluplus Micelles for Improving the Oral Bioavailability of Scopoletin and their Hypouricemic Effect In Vivo. *Acta Pharmacol. Sin.* **2017**, *38*, 424–433. [[CrossRef](#)]
11. Dian, L.; Yu, E.; Chen, X.; Wen, X.; Zhang, Z. Enhancing Oral Bioavailability of Quercetin Using Novel Soluplus Polymeric Micelles Nanoscale. *Res. Lett.* **2014**, *9*, 684.
12. Meister, A. Glutathione-Ascorbic Acid Antioxidant System in Animals. *J. Biol. Chem.* **1994**, *269*, 9397–9400. [[CrossRef](#)]
13. Kameyama, K.; Sakai, C.; Kondoh, S. Inhibitory Effect of Magnesium L-Ascorbyl-2-Phosphate (VC-PMG) on Melanogenesis In Vitro and In Vivo. *J. Am. Acad. Dermatol.* **1996**, *34*, 29–33. [[CrossRef](#)]
14. Palma, S.; Manzo, R.; Nostro, P.; Allemandi, D. Nanostructures from Alkyl Vitamin C Derivatives (ASCn): Properties and Potential Platform for Drug Delivery. *Int. J. Pharm.* **2007**, *345*, 26–34. [[CrossRef](#)]
15. Lan, H.H.; Yukitaka, K.; Shuji, A. Discoloration Kinetics of L-Ascorbyl 0-Palmitate Powders with Various Water Contents. *Food Sci.* **2007**, *13*, 7–12.
16. Moribe, K.; Maruyama, S.; Inoue, Y.; Suzuki, T.; Fukami, T.; Tomono, K.; Higashi, K.; Tozuka, Y.; Yamamoto, K. Ascorbyl Dipalmitate/PEG-Lipid Nanoparticles as a Novel Carrier for Hydrophobic Drugs. *Int. J. Pharm.* **2010**, *387*, 236–243. [[CrossRef](#)] [[PubMed](#)]
17. Takayama, R.; Inoue, Y.; Murata, I.; Kanamoto, I. Characterization of Nanoparticles Using DSPE-PEG2000 and Soluplus. *J. Colloids Interfaces* **2020**, *4*, 28. [[CrossRef](#)]
18. Dargie, H.J.; Dollery, C.T.; Daniel, J. Minoxidil in resistant hypertension. *Lancet* **1977**, *2*, 515–518. (In Japanese) [[CrossRef](#)]
19. Otomo, S. Hair Growth Effect of Minoxidil. *Folia Pharmacol.* **2002**, *119*, 167–174. [[CrossRef](#)] [[PubMed](#)]
20. Tanida, S.; Kurokawa, T.; Sato, H.; Kadota, K.; Tozuka, Y. Evaluation of the Micellization Mechanism of an Amphiphatic Graft Copolymer with Enhanced Solubility of Ipriflavone. *Chem. Pharm. Bull.* **2016**, *64*, 68–72. [[CrossRef](#)] [[PubMed](#)]
21. Yamaguchi, K.; Mitsui, T.; Aso, Y.; Sugibayashi, K. Structure-Permeability Relationship Analysis of the Permeation Barrier Properties of the Stratum Corneum and Viable Epidermis/Dermis of Rat Skin. *J. Pharm. Sci.* **2008**, *97*, 4391–4403. [[CrossRef](#)]
22. Takeuchi, H.; Terasaka, S.; Sakurai, T.; Furuya, A.; Urano, H.; Sugibayashi, K. Variation Assessment for in Vitro Permeabilities through Yucatan Micropig Skin. *Biol. Pharm. Bull.* **2011**, *34*, 555–561. [[CrossRef](#)] [[PubMed](#)]
23. Arce, F.J.; Asano, N.; See, G.L.; Oshizaka, T.; Itakura, S.; Todo, H.; Sugibayashi, K. Prediction of skin permeation and concentration of rhododendrol applied as finite dose from complex cosmetic vehicles. *Int. J. Pharm.* **2020**, *578*, 119186. [[CrossRef](#)]
24. Mishra, P.R.; Shaal, L.A.; Müller, R.H.; Keck, C.M. Production and Characterization of Hesperetin Nanosuspensions for Dermal Delivery. *Int. J. Pharm.* **2009**, *371*, 182–189. [[CrossRef](#)] [[PubMed](#)]
25. Tokudome, Y.; Uchida, R.; Yokote, T.; Todo, H.; Hada, N.; Kon, T.; Yasuda, J.; Hayashi, H.; Hashimoto, F.; Sugibayashi, K. Effect of Topically Applied Sphingomyelin-Based Liposomes on the Ceramide Level in a Three-Dimensional Cultured Human Skin Model. *J. Liposome Res.* **2010**, *20*, 49–54. [[CrossRef](#)] [[PubMed](#)]

- 
26. Inoue, Y.; Yoshimura, S.; Tozuka, Y.; Moribe, K.; Kumamoto, T.; Ishikawa, T.; Yamamoto, K. Application of Ascorbic Acid 2-Glucoside as a Solubilizing Agent for Clarithromycin: Solubilization and Nanoparticle Formation. *Int. J. Pharm.* **2007**, *331*, 38–45. [[CrossRef](#)]
  27. Kurata, T.; Nishikawa, Y. Chemical properties of Oxidized- L-ascorbic acid. *Biosci Biotechnol Biochem* **2003**, *77*, 1138–1139.